Neurobiology of Aging 150 (2025) 69–79

Contents lists available at ScienceDirect

Neurobiology of Aging

journal homepage: www.elsevier.com/locate/neuaging.org

Excitatory and inhibitory neurotransmitter alterations with advancing age and injury in the mouse retina

Katharina C. Bell [a,b,*], Vicki Chrysostomou [b], Markus Karlsson [c], Bryan W. Jones [d], Pete A. Williams [e,1], Jonathan G. Crowston [b,c,1]

[a] NHMRC Clinical Trial Centre, University of Sydney, 92-94 Parramatta Rd, Camperdown, NSW 2050, Australia
[b] Neuroscience and Behavioural Diseases and Eye-ACP, SERI/SNEC, Centre for Vision Research, Duke-NUS Medical School, 8 College Road, 169857, Singapore
[c] Save Sight Institute, University of Sydney, Sydney, NSW, Australia
[d] John Moran Eye Center, University of Utah School of Medicine, Salt Lake City, UT 84132, United States
[e] Department of Clinical Neuroscience, Division of Eye and Vision, St. Erik Eye Hospital, Karolinska Institutet, Stockholm, Sweden

ARTICLE INFO

Keywords:
Retinal ganglion cells
Retina
Metabolomics
Neurotransmitter
Glaucoma
Aging
Intraocular pressure

ABSTRACT

Increasing age and elevated intraocular pressure (IOP) are the two major risk factors for glaucoma, the most common cause of irreversible blindness worldwide. Accumulating evidence is pointing to metabolic failure predisposing to neuronal loss with advancing age and IOP injury. Many neurotransmitters are synthesized from endogenous metabolites and are essential for correct cell to cell signaling along the visual pathways. We performed detailed, small molecule metabolomic profiling of the aging mouse retina and further explored the impact of IOP elevation at different ages. The resultant metabolomic profiles showed clear discrimination between young and middle-aged retinas and these changes are accentuated following eye pressure elevation. Alterations in glutamate and Gamma-aminobutyric acid (GABA) related metabolites were the most apparent changes with advancing age with further reductions in GABA and related pathways after IOP elevation. These changes were further confirmed using immunohistochemistry and patch-clamp electrophysiological recording experiments.

1. Introduction

Glaucoma is the most common cause of irreversible blindness worldwide. The number of affected individuals is expected to increase to 112 million by 2040, consequent to increased life-expectancy in many countries (GBD, 2019 Blindness and Vision Impairment Collaborators; Vision Loss Expert Group of the Global Burden of Disease Study, 2021; Tham et al., 2014). Glaucoma is manifest by the selective loss of retinal ganglion cells (RGCs) that transmit the visual message from the retina to the brain. Advancing age and intraocular pressure (IOP) elevation are two leading risk factors for developing glaucoma (Quigley and Broman, 2006). Despite IOP lowering, vision loss can still progress and up to 20 % of patients progress to monocular blindness (Bengtsson et al., 2024). It is therefore likely that other factors play a role in the pathogenesis of glaucoma.

There is accumulating evidence that links metabolic failure with loss of RGCS. This includes disturbed glucose, pyruvate, and Nicotinamide adenine dinucleotide (NAD) metabolism in several experimental animal models as well as alterations in the metabolites of human tear and aqueous humor samples taken from primary open angle glaucoma patients (Baltan et al., 2010; Casson et al., 2021; Harder et al., 2020; Myer et al., 2020; Rossi et al., 2019; Tribble et al., 2021; Williams et al., 2017). In addition to playing an important role in cell energy supply, metabolites are also important constituents of neurotransmitters, such as glutamate or Gamma-aminobutyric acid (GABA) that are essential for neurotransmission along the visual pathway.

We have previously demonstrated impaired functional recovery and increased neuronal loss in response to short term elevation of IOP. A significant impairment in recovery and elevated vulnerability to repeat IOP elevations were already clearly manifest in middle aged mice (12 months of age) compared to young (3 months of age) mice (Chrysostomou et al., 2024; Crowston et al., 2015; Fry et al., 2018; Kong et al., 2009). Whereas full functional recovery is seen in young mice (3 months of age) by 7- days after a single IOP elevation, delayed and

* Correspondence to: NHMRC Clinical Trial Centre, University of Sydney, Camperdown NSW 2050, Australia.
E-mail addresses: katharina.bell@sydney.edu.au (K.C. Bell), v.chrysostomou@duke-nus.edu.sg (V. Chrysostomou), erikmarkus.karlsson@sydney.edu.au (M. Karlsson), u0060967@umail.utah.edu (B.W. Jones), pete.williams@ki.se (P.A. Williams), jonathan.crowston@sydney.edu.au (J.G. Crowston).
[1] Contributed equally

https://doi.org/10.1016/j.neurobiolaging.2025.03.004
Received 26 July 2024; Received in revised form 23 January 2025; Accepted 2 March 2025
Available online 8 March 2025

incomplete (to 85 % of baseline) recovery is seen in 12 months of age mice. Older, 24 months of age mice do not recover function following a similar IOP challenge (Chrysostomou et al., 2024, 2014; Crowston et al., 2015). The mechanisms that underpin these dramatic differences in RGC response are still to be fully elucidated.

To further understand the underlying cellular mechanisms associated with these differences in the capacity to recover function we conducted a detailed analysis of the retinal metabolome to explore metabolic changes with age and the overlying impact of IOP elevation. We additionally explored a publicly available dataset derived from the DBA/2J mouse, which suffers sustained elevation of IOP and RGC loss. We hereby present a detailed, selected-small molecule metabolomics profile of the aging mouse retina along and additionally document the effect of superimposed injury. These data point to both aging and IOP elevation having a significant impact on glutamate and GABA signaling.

2. Materials and methods

2.1. Animal strain and husbandry

All animal procedures conformed to the ARVO (Association for Research in Vision and Ophthalmology) Statement for the Use of Animals in Ophthalmic and Vision Research. IOP elevation experiments for metabolomics and immunohistochemistry were approved by the SingHealth Institutional Animal Care and Use Committee (2019/SHS/1534). Male and female C57BL/6J mice at 3 and 12 months of age were purchased from InVivos Pte Ltd, Singapore, and housed at the SingHealth Experimental Medicine Centre (Academia, Singapore) in a temperature- (22 ± 1 °C), light- (12 h light, 12 h dark) and humidity-controlled (30–40 %) environment with free access to food and water. Prior to procedures, animals were anesthetized by intraperitoneal injection of ketamine:xylazine (80:10 mg/kg). Topical proxymetacaine (0.5 % Alcaine, Alcon Laboratories) and tropicamide (1 % Mydriacyl, Alcon Laboratories) were instilled to induce local anesthesia and pupil dilation respectively. Animal core body temperature was maintained at 37.0 ± 0.5°C on a heated platform throughout experiments. IOP elevation was performed on both the 3 months of age and 12 months of age mice (N per group = 8). Experiments for electrophysiology were performed at the Florey Institute, Melbourne, under the guidelines of the Australian Code of Practice for the Care and were approved by The Florey Animal Ethics Committee (18–112-FINMH). Three months of age B6.Cg-Tg(Thy1-YFP)HJrs/J mice (Stock No: 003783; The Jackson Laboratory, USA), hereafter termed Thy1-YFP mice, were maintained on a 12-hour light/dark cycle and housed in a PC2 facility with ad libitum access to food and water (N per group = 4–6). Male and female mice were used for all experiments.

2.2. Intraocular pressure elevation

RGC injury was induced by short-term elevation of IOP, a well-characterized non-ischemic insult that has been described in detail (Crowston et al., 2015; Kong et al., 2009). For this, the anterior chamber of the mouse eye was cannulated with a 50 μm borosilicate needle connected via polyethylene tubing to a syringe mounted on a motorized pump (PHD Ultra CP; Harvard Apparatus, Massachusetts, USA) and a pressure transducer (Transpac IV, Abbott Critical Care Systems, Sligo, Ireland). The syringe and tubing were filled with sterile-filtered endotoxin-tested Hanks' balanced salt solution reservoir (HBSS, JRH Biosciences, Lenexa, KA, USA). HBSS was chosen as the fluid in the pressure column as its concentrations of salts and ions show a close approximation to aqueous humor. The pump was calibrated to drive fluid to maintain a constant pressure within 1 mmHg of the target. Resting IOP was recorded immediately after cannulation of the anterior chamber before IOP was elevated to 50 mmHg for 30 min. The contralateral eye served as an untreated control. A schematic of the model and experimental design has been depicted in the graphical abstract.

2.3. Small molecule metabolomics

Three days post-IOP injury of the 3 months of age and 12 months of age mice, the retina from the injured eye as well as the contralateral eye were immediately extracted in ice cold HBSS, dried and snap frozen. Tissues were stored at −80 °C until shipment on dry ice to the Swedish Metabolomics Centre. Measurements were performed as described previously (Tribble et al., 2021). Briefly, 200 μL extraction buffer (80/20 v/v methanol: water) including internal standards and 1 tungsten bead were added to each tube. After shaking (30 Hz for 3 min) and centrifugation (+4 °C, 14,000 rpm for 10 min), 170μL supernatant evaporated to dryness and the samples were stored at −80 °C until analysis. Small aliquots of the remaining supernatants were pooled and used to create quality control (QC) samples. Re-suspension and measurements of the samples were performed as detailed in Canovai et al. (Canovai et al., 2023). Before randomized batch analysis, the samples were re-suspended in 10 + 10 μL methanol and elution solvent A. Each batch of samples was first analysed in positive mode and then the instrument was switched to negative mode and a second injection of each sample was performed. Chromatographic separation was performed on an Agilent 1290 Infinity UHPLC-system (Agilent Technologies, Waldbronn, Germany). 2 μL of each sample were injected onto an Atlantis Premier BEH-Z-HILIC VanGuard FIT (1.7 μm, 2.1 x 50 mm) column (Waters Corporation, Milford, MA, USA) held at 40 °C. The HILIC gradient elution solvents were A) H2O, 10 mM ammonium formate, 5μM Medronic acid, pH 9, B) 90:10 Acetonitrile: H2O, 10 mM ammonium formate, pH 9 and 5 μM Medronic acid. Chromatographic separation was achieved using a linear gradient (flow rate 0.4 mL/min): min 0 = 90 % B, min 6 = 80 % B; min 9.5 = 20 % B, min 11 = 90 % B. The flow rate was increased to 0.7 mL/min for 2 min, held at this rate for 0.5 min, and then reduced to 0.4 mL/min for 0.5 min before the next injection. The compounds were detected with an Agilent 6546 Q-TOF mass spectrometer equipped with a jet stream electrospray ion source operating in positive or negative ion mode. The reference ions purine (4 μM) and HP-0921 (1 μM) were infused directly into the MS at a flow rate of 0.05 mL min-1 for internal calibration. Gas temperature was set to 150°C, the drying gas flow to 8 L min-1 and the nebulizer pressure 35 psi. Sheath gas temp was set to 350°C and the sheath gas flow 11 L min-1. The capillary voltage was set to 4000 V in both positive and negative ion mode. The nozzle voltage was 300 V. The fragmentor voltage was 120 V, the skimmer 65 V and the OCT 1 RF Vpp 750 V. The collision energy was set to 0 V. The m/z range was 70–1700, and data was collected in centroid mode with an acquisition rate of 4 scans s-1. MSMS analysis was run on the QC samples for identification purposes. All data pre-processing was performed using the Agilent MassHunter Profinder version B.10.0 SP1 (Agilent Technologies Inc., Santa Clara, CA, USA). The data pre-processing was performed in a targeted fashion. A pre-defined list of metabolites commonly found in plasma and serum were searched for using the Batch Targeted feature extraction in MassHunter Profinder. An-in-house LC-MS library built up by authentic standards run on the same system with the same chromatographic and mass-spec settings, were used for the targeted processing. One hundred low molecular weight metabolites that could be certified with standards were detected. The quantification of the metabolites was calculated as area under the curve of the mass spectrometry peak and normalized to an internal standard for negative and positive runs. Data were analysed and graphs were made using MetaboAnalyst [version 6.0;] and R (Xia et al., 2009; Xia and Wishart, 2011). All data were normalised by the sample median and subjected to auto scaling (van den Berg et al., 2006). Principal component analysis (PCA) was performed in with Metaboanalyst. Comparisons between groups were analysed by two-sample t-tests with an adjusted p value using a cutoff of 0.05 considered significant. Over Representation Analysis (ORA) was implemented using the hypergeometric test available with Metaboanalyst to evaluate whether a particular metabolite set is represented more than expected by chance within the given compound list. One-tailed p values are

provided after adjusting for multiple testing. Receiver operating curves were calculated with the standard settings in Metaboanalyst (linear support vector machines (SVM)). Quantitative pathway analysis was performed using the *Mus musculus* KEGG library in MetaboAnalyst and a background metabolome of all detected metabolites from the same samples.

2.4. Immunohistochemistry

GABA immunoreactivity of the control and injured retina of 3 months of age mice at day 3 after IOP elevation was performed as previously described in detail (Marc et al., 1995) (N = 4/group). Briefly, day 3 after IOP injury both eyes were removed and rapidly fixed in 1 % paraformaldehyde, 2.5 % glutaraldehyde, 3 % sucrose, 0.01 % CaCl2, in 0.1 M phosphate buffer, pH 7.4. Eyes were dehydrated and embedded in epoxy resin, followed by sectioning at 250 nm onto 12-spot Teflon-coated slides. Samples were probed with IgGs targeting GABA (anti-GABA IgG, AB_2532061, Signature Immunologics, 1:50) and cellular Retinaldehyde binding protein 1 (CRALBP) (anti-CRALBP IgG, AB, AB_2314227, 1:400; gift of Dr. John Saari). Primary IgG for GABA and CRALBP was detected with goat anti-rabbit IgGs adsorbed to 1 nm gold particles and visualized with silver intensification. Light microscopic images were captured as 12-bit 1936 pixel × 1456 line frames under constant flux light with feedback regulation and fixed CCD camera gain and gamma, as described previously (Marc and Jones, 2002). Analysis of the GABA signal was performed in a masked fashion using the manual cell counter in ImageJ. From each retinal section all GABA positive cells were subdivided to being either GABA-hi or GABA-lo. All cells were counted, and the length of the retinal section was measured. The number of either GABA-hi or GABA-lo cells/182μm (1000 pixels) were calculated and a Kruskal-Wallis test was performed with GraphPad Prism (Version 10.2.1) with an alpha of 0.05 to determine if there were any statistically significant measurements.

3. Whole-cell patch-clamp electrophysiology

3.1. Retinal preparation

Eyes were removed and transferred into cold dissecting solution (125 mM Choline Cl, 2.5 mM KCl, 0.4 mM CaCl2, 6 mM MgCl2, 1.25 mM NaH2PO4, 26 mM NaHCO3 and 20 mM D-glucose) and saturated with 95 % O2/5 % CO2. The cornea was immediately punctured with a 23 G needle to allow oxygenation. The retina was dissected out, hemisected and the vitreous removed. Retinal hemisections (A1420; Sigma Aldrich, USA) saturated with 95 % O2/5 % CO2 for one hour at room temperature.

3.2. Whole-cell patch-clamp electrophysiology

Retinal hemisections were transferred to a recording chamber with the RGC layer facing up and set in place with a harp. The recoding chamber were placed on an upright microscope (Slicescope Pro 1000; Scientifica, UK) and perfused with AMES medium (22.6 mM NaHCO3) saturated with 95 % O2/5 % CO2 at room temperature and at a rate of 2 mL/min. RGCs and bipolar cells were identified visually using a fluorescence lamp under a 40x water-immersion objective and a CCD camera.

3.3. Electrodes

Glass electrodes (BF150–110–10 and BF150–86–7.5HP; Sutter Instruments, USA) were pulled using a Flaming Brown micropipette puller (Model P-1000, Sutter instruments, USA) to produce a resistance of 0.5–1 MΩ (stimulating electrodes) and 4–7 MΩ (recoding electrodes. Silver wire was wrapped around the glass electrode and connected via an insulated wire to a stimulating box. Glass electrodes were painted in silver-chloride paint. Stimulating electrodes were filled with AMES media (22.6 mM NaHCO3), fastened in a microelectrode holder containing a silver chloride coated electrode. Positive pressure was added to the stimulating electrode, which was then placed within the bipolar cell layer. Recording electrodes were placed within the ganglion cell layer above the stimulating electrode. Synaptic currents were recorded with electrodes containing: 135 mM CsMeSO4, 8 mM NaCl, 10 mM HEPES, 2 Mg2ATP, 0. mM 3 Na3GTP, 7 Phosphocreatine, 10 EGTA (pH 7.3).

3.4. Inhibitory postsynaptic recordings (IPSC)

Patch-clamp recordings were made in current clamp mode using PatchStar micromanipulators (Scientifica, UK) and Acon Multiclamp 700B patch-clamp amplifier (Molecular Devices, USA). Data were acquired using pClamp software (v10; Molecule Devices, USA) with a sampling date of 50 kHz and low pass bessel filtered at 10 kHz (Digidata, 1440a; Axon).

IPSCs were evoked using a single 0.5 mA, 1 ms pulse repeated 10 times every 10 s (Digital Isolator, Model BIN8–9V; Getting Instruments, USA). Spontaneous inhibitory postsynaptic currents (sIPSCs) were recorded using a 2-minute-long gap-free protocol. Evoked inhibitory postsynaptic currents (eIPSCs) and sIPSCs were recorded by holding the retinal ganglion cells at + 10 mV172.

3.5. Data analysis

eIPSC recordings were analysed using AxoGraph software (Berkeley, USA). Cells with an access resistance of < 40 MΩ were analysed. All 10 recordings had their baseline subtracted from 0–250 ms. The peak eIPSC amplitude was detected from 500–700 ms and the peak shape was analysed to determine eIPSC onset, rise time and decay time. eIPSC amplitude, onset, rise time and decay time were averaged for all 10 recordings per cell.

sIPSCs were analysed using AxoGraph software (Berkeley, USA). Recordings were first divided into episodic chunks of 12 s. Traces were then be filtered using a sharp low pass filter at 5 kHz. A template function for sIPSCs was be defined with a baseline of 10 ms, template length of 20 ms, amplitude of 30 pA, rise time of 4 ms and decay time of 10 ms. Events were detected at a threshold of 2 x standard deviation. Cumulative frequency was extracted for the detected events and saved. All events with an amplitude over −100 pA were removed.

3.6. Statistical analysis

All data were imported into Prism (GraphPad Software, USA) for statistical analysis. Outliers were identified using the ROUT outlier's method to identify up to 2 outliers (Q = 1 %) and excluded from the analysis. One-way ANOVA (alpha = 0.05) and subsequent Tukey's multiple comparisons test was used to compare the mean of each group with the mean of the control group. Descriptive statistics were reported as (mean ± standard deviation, number of values).

4. Additional IOP injury dataset

Short term IOP elevation results in a reversible loss of the pSTR changes with limited RGC loss (Chrysostomou and Crowston, 2013; Crowston et al., 2015). To understand in greater detail the effect of IOP elevation that precedes RGC cell death, we also analyzed a publicly available metabolomics dataset using the DBA/2J mouse model (Harder et al., 2020). At timepoint of the measurement of retina from C57BL/6J (B6), DBA/2J (D2; glaucoma), and DBA/2J-*Gpnmb*^{R150X} (D2-Gpnmb+; control) mice were 9 months of age. DBA/2J mice at this timepoint had developed ongoing elevated IOP, however without RGC death, allowing for the analysis of pre-degenerative metabolomic changes in the retina. Measurements of 9 D2 mice and 10 D2-Gpnmb+ mice were included from the publicly available dataset. Detailed methods are described in

the original study (Harder et al., 2020). Analysis and statistics were performed with Metaboanalyst [version 6.0] as described above.

5. Results

5.1. Advancing age alters the metabolomic profile of the mouse retina

One hundred low molecular weight metabolites were detected with high accuracy and measured in both the non-injured 3 months of age retina and 12 months of age non-injured retina **(raw data, processed and annotated data is available from Zenodo, doi: 10.5281/zenodo.14723294)**. Of these, 14 metabolites were significantly increased in 12 months of age retinas and 3 metabolites were significantly decreased in comparison to retinas from young mice (Fig. 1A). Some of these metabolites, such as indoxyl sulfate and hippuric acid are known to increase with age in other human and rodent tissues and serum (Schnackenberg et al., 2007; Tan et al., 2023; Wyczalkowska-Tomasik et al., 2017), and 3-methylhistidine has previously been demonstrated to be increased in the aging retina (Wang et al., 2018) further validating our approach. Pathways known to be involved in the aging process such as the nicotinate and nicotinamide metabolism (Fig. 1B) (Covarrubias et al., 2021) were enriched in the KEGG enrichment analysis as well as both the degradation and biosynthesis pathways of the branch chain amino acids valine, leucine, and isoleucine. These amino acids are involved in a multitude of metabolic pathways as well as the regulation of glutamate levels in the CNS (Zhang et al., 2023). Of the various exploratory Receiver Operating Characteristic (ROC) curves calculated, model 3 using 10 features for discrimination resulted in the highest predictive accuracy of 95.3 % (Suppl. Fig. 1A and B) and showed high specificity and sensitivity of the measured metabolites with aging (area under the curve = 0.987) (Fig 1). This also resulted in high predictability of middle-aged versus young based on the metabolic signature (Fig. 1D).

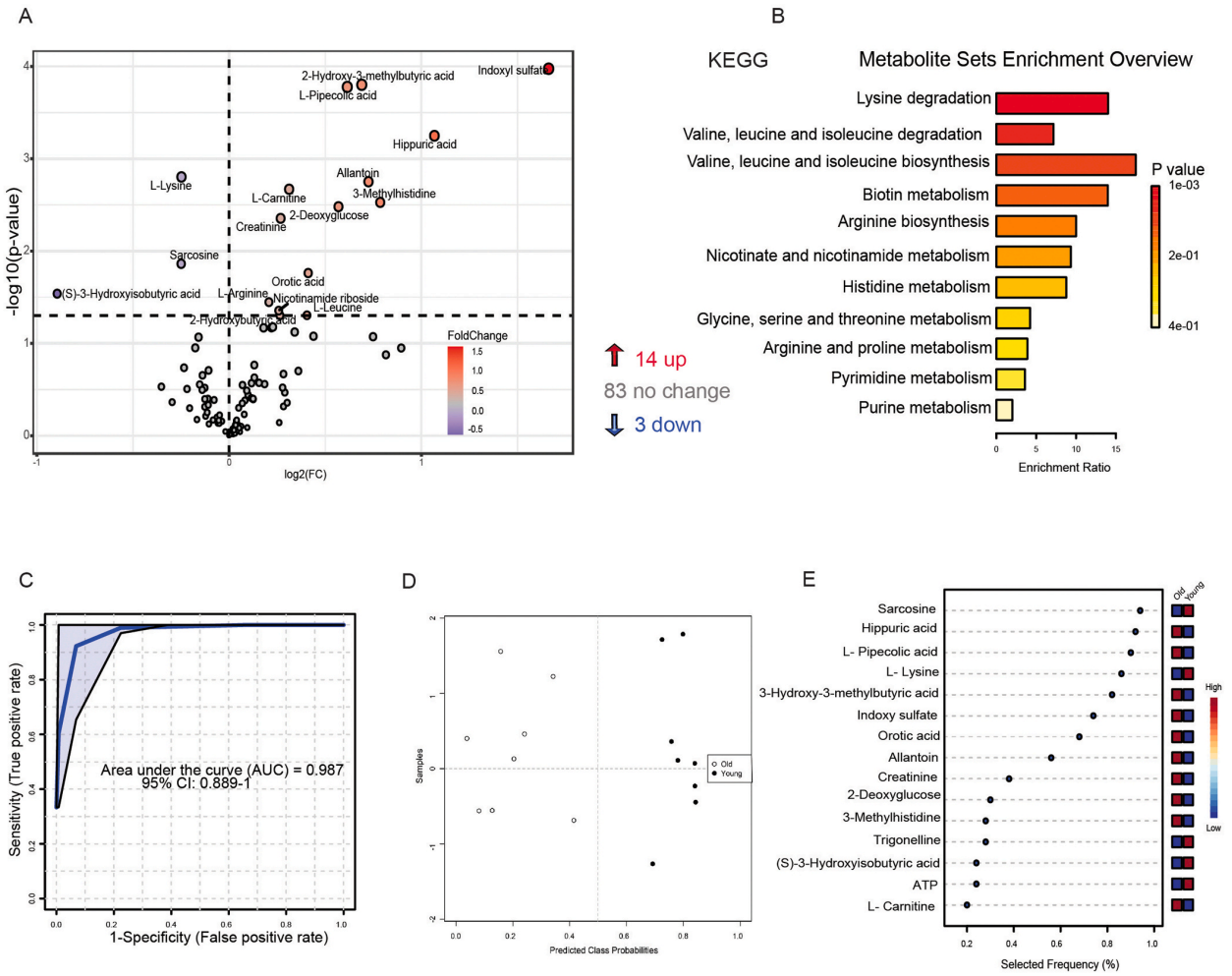

Fig. 1. Metabolic signatures with aging. A: Whole retina samples of non-injured retina from 3- and 12 months of age mice underwent metabolic profiling. A total of 100 metabolites were identified. Volcano plot indicating the number and the increase/decrease of significantly changed metabolites in 12 months of age non-injured retinae in comparison to 3 months of age non-injured retinae (p-value < 0.05, red = increased, blue = decreased). Of the 100 measured metabolites 14 were increased and 3 were decreased in retina from 12 months of age mice in comparison to retina from 3 months of age animals. N = 8 mice/group. B: Summary Plot for Kyoto Encyclopedia of Genes and Genomes (KEGG) Over Representation Analysis (ORA) metabolites demonstrates significant pathway enrichment of pathways related to Lysine degradation and valine, leucine and isoleucine degradation and biosynthesis C: The calculated exploratory Receiver Operating Characteristic Curve (ROC) calculated with 10 features (model 3) shows high specificity and sensitivity of the measured metabolites with aging (Area under the curve = 0.987). The 95 percent confidence interval is shown as a band around the ROC curve. D: Plot of predicted class probabilities for all samples using a single biomarker model. The classification boundary is at the center (x = 0.5, dotted line). E Plot of the most important features of a selected model ranked from most to least important. 2 of the most relevant metabolites discriminating between old and young are relevant for intraretinal synaptic signaling.

Calculation of the most relevant metabolites in the biomarker model for discrimination between middle-aged and young mice were metabolites involved in intraretinal synaptic signaling such as sarcosine and L-lysine (Fig. 1E).

5.2. Effect of IOP injury on the retinal metabolome in 3 months of age mice

Metabolite profiles demonstrated clear differences among IOP-injured and non-injured retina. These differences are shown in the principal component analysis and ROC analysis (Fig. 2A and B). Multiple ROC curves were calculated and based on the predictive accuracies with different features (Suppl. Fig. 2A, B and C), we chose model number 3 that used 10 features for discrimination between the samples for the PCA and ROC curve (Fig. 2A and B). Out of the 100 measured metabolites, 18 were up-regulated and 18 were down-regulated in retina of young animals 3 days after IOP injury (Fig. 2C) and KEGG pathway analysis (Fig. 2D) revealed enrichment of pathways related to retinal neurotransmission including arginine and proline metabolism, glycine, serine and threonine metabolism and alanine, aspartate and glutamate metabolism. Guanidoacetic acid and 4-guanidobutanoic acid were among the most significantly up-regulated metabolites in the injured and also among the most relevant metabolites to discriminate between injured and non-injured retina (Guanidoacetic acid: Log2(FC)= 1.16, -Log10(p-value) = 7.0; 4-guanidobutanoic acid: Log2(FC)= 1.04, -Log10(p-value) = 5.6) (Fig. 2A, E).

5.3. Effect of IOP injury on the retinal metabolome of 12 months of age mice

Differences in the metabolome of non-injured and injured retina were less obvious in the middle-aged mice. The calculated principal component analysis was based on model 3 (Suppl. Fig. 3A and B) and shows no or minimal discrimination between the injured middle-aged

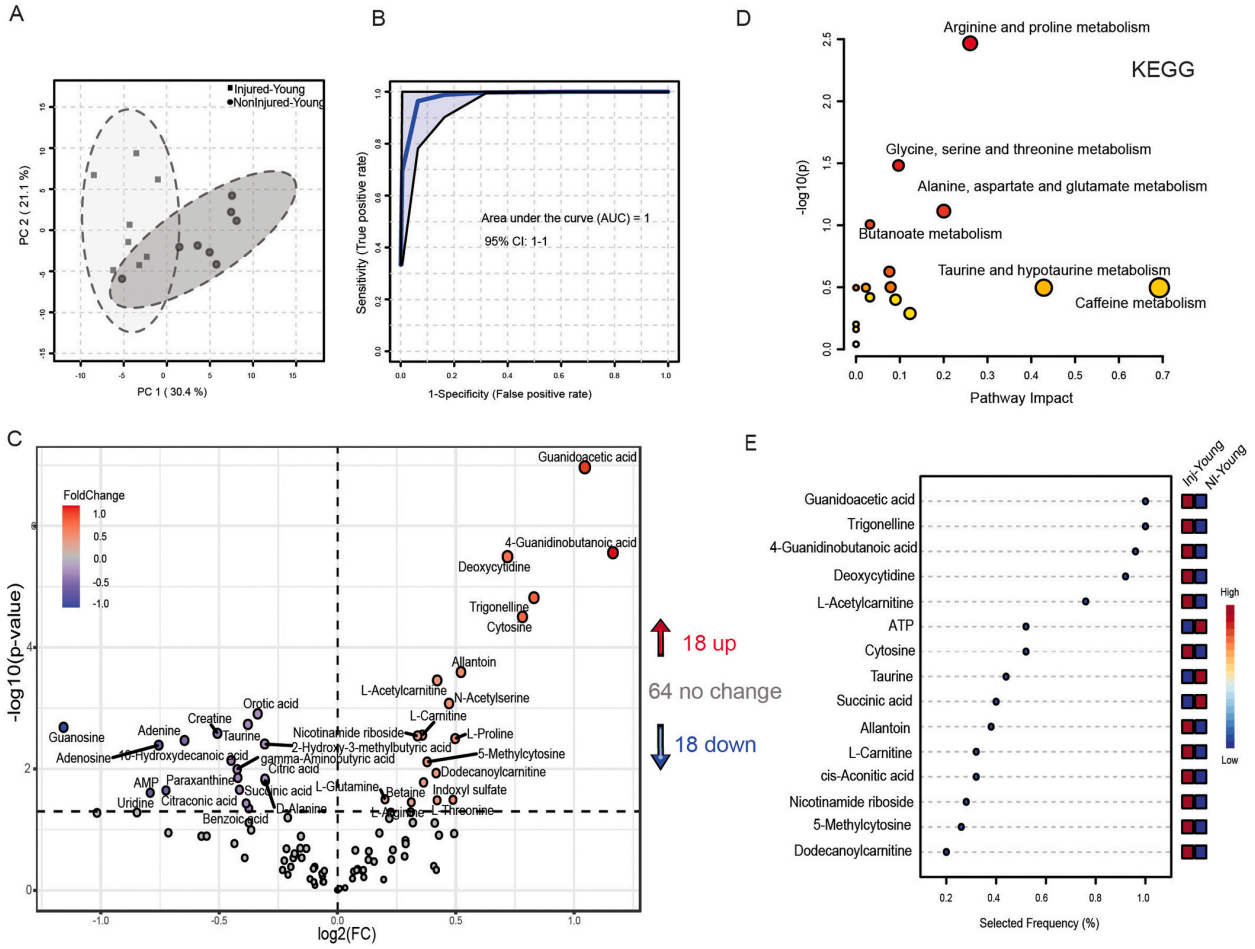

Fig. 2. Metabolic signatures in retina of 3 months of age mice after IOP injury. A: The calculated principal component analysis (PCA) shows good discrimination between injured and non-injured retina in the 3 months of age animals (squares represent the injured 3- months of age retina, dots represent the non-injured 3 months of age retina). N = 8 mice/group. B: The calculated exploratory Receiver Operating Characteristic Curve (ROC) calculated with 10 features (model 3) shows high specificity and sensitivity of the measured retinal metabolites with injury in 3 months of age mice (Area under the curve = 1). The 95 percent confidence interval is shown as a band around the ROC curve. C: Whole retina samples of injured (single IOP challenge) and non-injured retina from 3 months of age mice underwent metabolic profiling. Of the total of 100 identified metabolites, 18 were up-regulated and 18 were down-regulated in retinae of young animals 3 days after a single IOP elevation injury, as demonstrated in the volcano plot (FDR < 0.05, red = increased, blue = decreased). D: Kyoto Encyclopedia of Genes and Genomes (KEGG) pathway analysis of metabolites demonstrates significant pathway enrichment of pathways related to neurotransmission such as Arginine and proline metabolism, Glycine, serine and threonine metabolism and Alanine, aspartate and glutamate metabolism. Another enriched pathway is the taurine and hypotaurine metabolism. E: Plot of the most important features of a selected model (Model 3) ranked from most to least important. Guanidoacetic acid is one main metabolite in this model to discriminate between injured and uninjured retina and is increased in injured retina after IOP a single IOP in 3 months of age animals.

retinal samples versus the non-injured samples (Fig. 3A and suppl. Fig. 3C). This is also reflected in the calculated ROC curve (Fig. 3B). Of the 100 measured metabolites, 8 were up-regulated and 11 were down-regulated in retina of 12 months of age animals 3 days after a single IOP elevation injury (Fig. 3C) and KEGG pathway analysis (Fig. 3D) of these metabolites again revealed enrichment of pathways related to retinal neurotransmission such as arginine and proline metabolism, glycine, serine and threonine metabolism and phenylalanine, tyrosine and tryptophan biosynthesis. Cytidine and succinic acid are among the metabolites that were most frequently used to discriminate the injured samples from the non-injured samples (Fig. 3E). Cytidine plays a role in neuronal-glial glutamate cycling and can decrease glutamate and glutamine levels in the CNS and thus glutamate induced excitotoxicity (Mir et al., 2003; Yoon et al., 2009) and succinic acid is involved in the GABA shunt, which connects the tricarboxylic acid (TCA) cycle to GABA and glutamate metabolism (Schousboe et al., 2013).

5.4. GABA decreased after IOP elevation in young and middle-aged mice

Of the 36 metabolites differently regulated in the retina of 3 months of age mice after injury and the 19 metabolites differently regulated in the 12 months of age injured retina, 13 metabolites were detected in both the middle-aged and the young retina after injury (Fig. 4A). All these metabolites showed the same direction of change in both age groups after a single short-term IOP elevation (Fig. 4A). GABA, the main inhibitory neurotransmitter in the retina was decreased after injury in both the middle-aged and the young mice and in addition, shows a general decrease in signal intensity with aging in the non-injured retina (Fig. 4B). Taurine, which is known to promote neuroprotection of RGCs after injury (Froger et al., 2012), was also decreased after injury in both the middle-aged and the young (Fig. 4B). Further investigation of GABA-positive cells in the retina was performed with immunohistochemistry. As expected, diffuse GABA staining was localized in the IPL and GABA staining of cell bodies was found in the INL and GCL of the retina. As CRALBP stains Mueller cells and the retinal pigment epithelium (RPE), it is shown here to allow the reader to localize the GABA

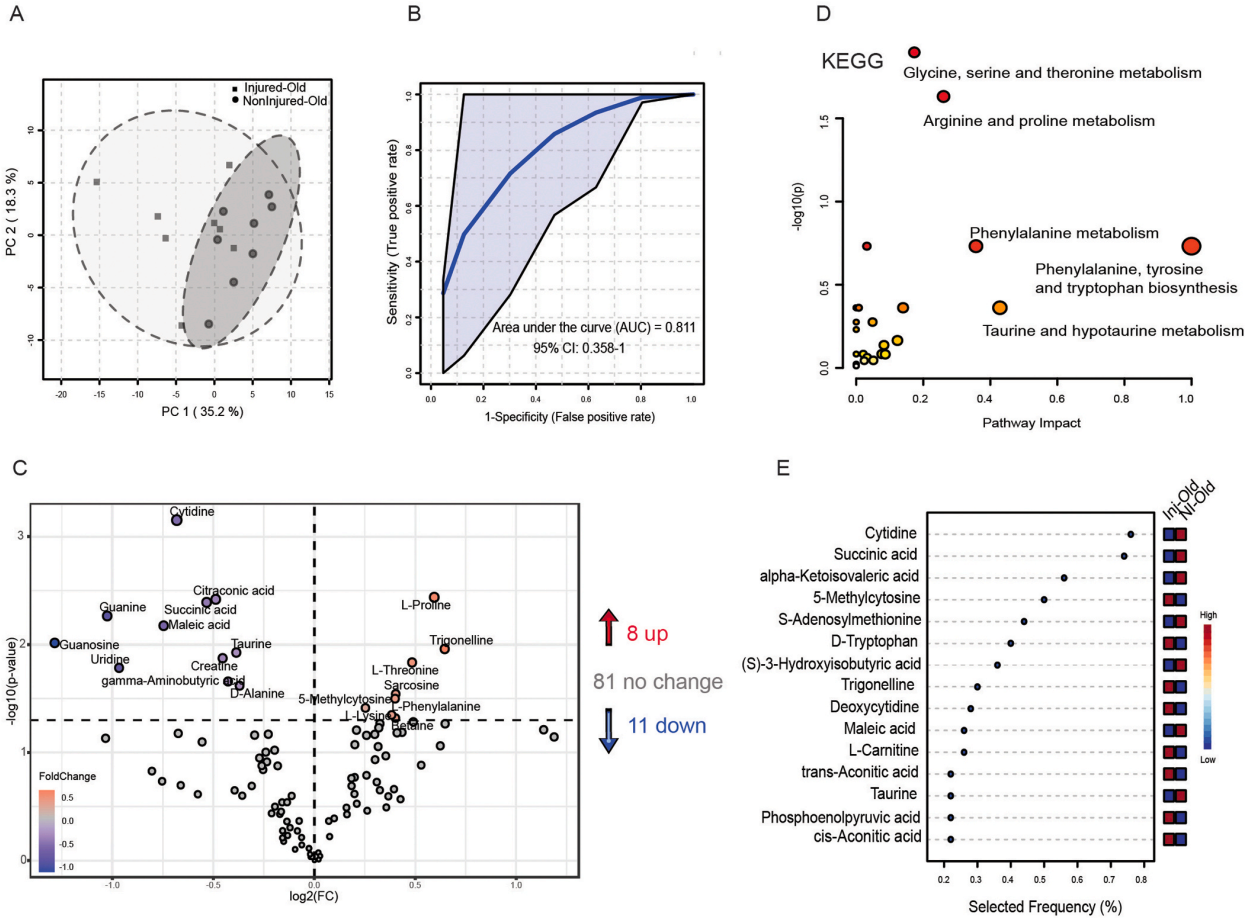

Fig. 3. Metabolic signatures in retina of 12 months of age mice after IOP injury. A: The calculated principal component analysis (PCA) fails to demonstrate discrimination between injured and non-injured retina in the 12 months of age animals (squares represent the injured 12 months of age retina, dots represent the non-injured 12 months of age retina). N = 8 mice/group. B: The calculated exploratory Receiver Operating Characteristic Curve (ROC) calculated with 10 features (model 3) shows lower specificity and sensitivity of the measured metabolites in 12 months of age retina after IOP elevation injury (Area under the curve = 0.811). The 95 percent confidence interval is shown as a band around the ROC curve. C: Whole retina samples of injured (single IOP challenge) and non-injured retina from 12 months of age mice underwent metabolic profiling. Of the total of 100 identified metabolites, 8 were up-regulated and 11 were down-regulated in retinae of old animals 3 days after a single IOP elevation injury, as demonstrated in the volcano plot (FDR < 0.05, red = increased, blue = decreased). D: Kyoto Encyclopedia of Genes and Genomes (KEGG) pathway analysis of metabolites demonstrates significant pathway enrichment related to neurotransmission and pathways related to Phenylalanine, tyrosine and tryptophan biosynthesis as well as taurine and hypotaurine metabolism. E Plot of the most important features of a selected model (Model 3) ranked from most to least important.

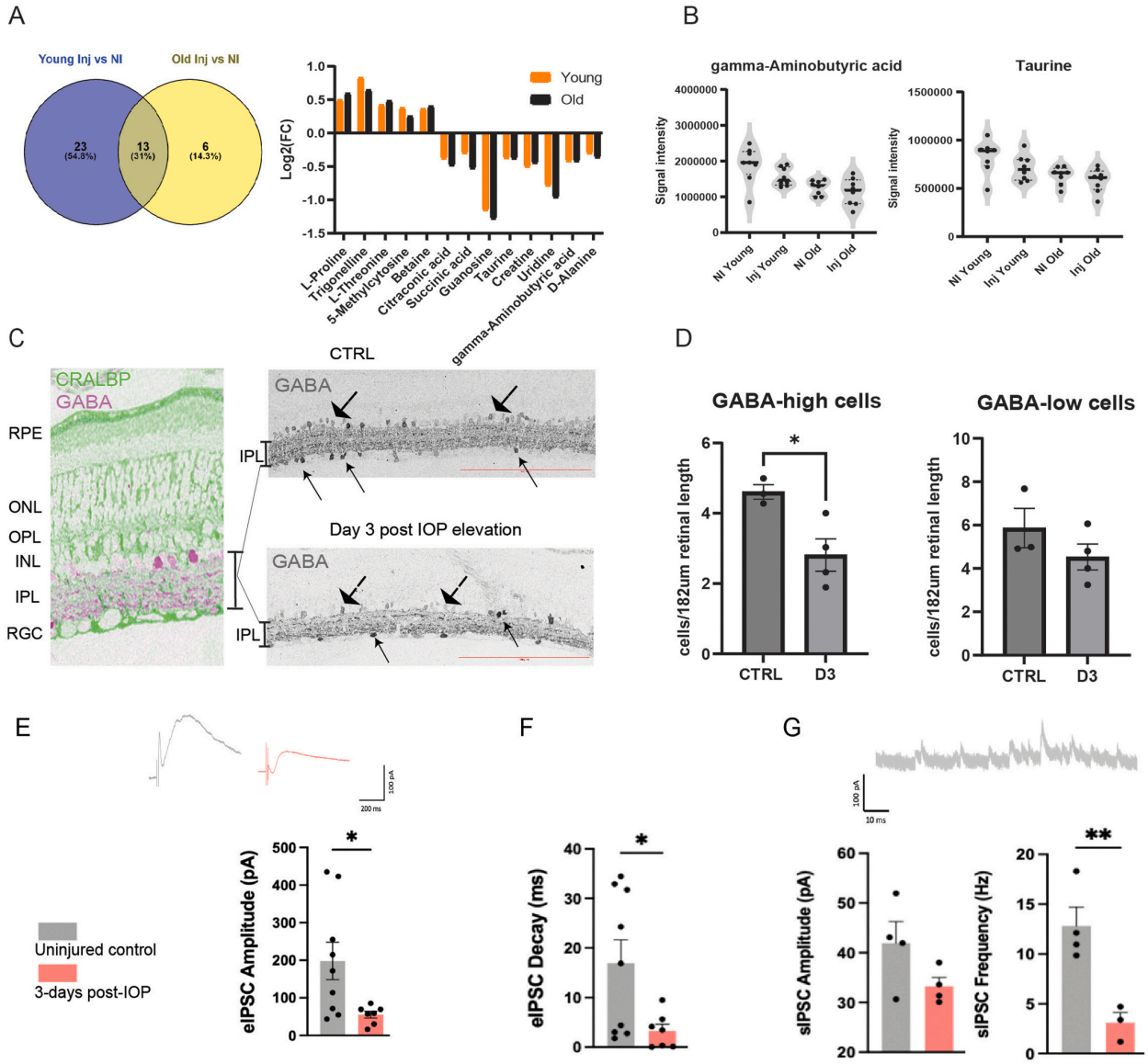

Fig. 4. Comparison of injury response in both young and middle-aged mice. A: 36 metabolites were significantly differently regulated in the retina of 3 months of age (young) mice after injury in comparison to the non-injured 3 months of age retina, whereas 19 metabolites were significantly differently regulated in the 12 months of age (old) injured retina in comparison to the 12 months of age non-injured control. Of these metabolites, 13 metabolites were found to be differently regulated in both the old and the young retina after injury. All these metabolites showed the same mode of change (increased or decreased levels) in the 12 months of age (black) and the 3 months of age (orange) retina after a single short term IOP elevation injury. N = 8 mice/group. B shows the signal intensity of GABA and Taurine, which are both found in significantly lower levels after IOP injury in the retina of 3 months of age and 12 months of age mice Violin plots show the non-normalized signal intensities. The black bar shows the median, the dotted lines show the 1st and the 3rd quartile. C shows localization of GABA immunoreactivity within the retina. CRALBP staining (green) highlights especially Mueller cells and the retinal pigment epithelium and allows to identify the different retinal layers. GABA immunoreactivity (purple) is seen in the IPL, INL and RGC layer. Exemplary grey scale images of GABA immunoreactivity in the CTRL and at Day 3 after IOP elevation are shown on the right. Arrows with small arrowheads point towards GABA-hi cells and arrows with large arrowheads point towards GABA-lo cells. Scale bar represents182µm D shows the GABA-hi and the GABA-lo cell numbers/182µm in the CTRL and Day-3 post-IOP elevation retina (D3) (* $p < 0.05$). N = 3 mice/group. E Example traces of eIPSC recordings from 3 months of age mice. eIPSC traces from uninjured controls and 3-days post IOP elevation. Scale = 200 ms x 100 pA. Quantification of the eIPSC amplitude demonstrates a significant reduction in IPSC amplitude 3-days post IOP elevation compared to controls (* $p < 0.05$). F Quantification of the eIPSC decay time demonstrates a significantly faster IPSC decay 3-days post IOP elevation compared to controls (* $p < 0.05$). G Example traces of spontaneous IPSC recordings from retinal ganglion cells in 3 months of age mice. sIPSCs were recorded 3-days post IOP elevation as well as from uninjured controls. Scale = 10 ms x 100 pA. Quantification of sIPSC amplitude demonstrates no significant change following IOP elevation ($p > 0.05$). Quantification of sIPSC frequency demonstrates a significant decrease in IPSC frequency 3-days post IOP elevation compared to controls (** $p < 0.01$). N = 4–6 mice/group.

staining within the retina (Fig. 4C left). In both the non-injured control retina and at day 3 after IOP elevation, cells containing high (hi) amounts of GABA (darker cells) and cells containing lower (lo) amounts of GABA were present (Fig. 4C right). GABA-hi and GABA-lo cells were counted in a masked fashion and calculated as cells per 182μm. Retinas at day 3 after IOP elevation injury shows a significant 40 % decrease in GABA-hi cells (CTRL mean value 4.6, SD 0.36, D3 mean value 2.8, SD 0.9; p-value <0.05) and a trend of decrease in the GABA-lo cells (CTRL mean value 5.8, SD 1.6, D3 mean value 4.5, SD 1.2) (Fig. 4D). GABA is the main inhibitory neurotransmitter in the retina. To study inhibitory synapse function in the retina, we therefore performed whole-cell patch-clamp electrophysiology to measure the evoked and spontaneous inhibitory potentials in the non-injured control retina as well as retina at day 3 after IOP elevation in 3 months of age mice. eIPSC (evoked inhibitory postsynaptic current) amplitude decreased significantly 3-days post IOP elevation compared to uninjured controls ($P = 0.029$; control 198.3 ± 149.5 pA, $n = 9$ cells; 3-days post IOP elevation $55.25.1 \pm 24.04$ pA, $n = 7$ cells) (Fig. 4E). As eIPSC amplitude was reduced following IOP elevation in 3 months of age mice, we also investigated the effects of IOP elevation on eIPSC kinetics. eIPSC onset (control 539.4 ± 2.95 ms, $n = 9$ cells; 3-days post IOP elevation 543.8 ± 6.326 ms, $n = 7$ cells) and rise time (control 3.39 ± 2.32 ms, $n = 7$ cells; 3-days post IOP elevation 3.13 ± 1.69 ms, $n = 7$ cells) were both unchanged at day 3 after IOP elevation. However, eIPSC decay was significantly faster day 3 after IOP elevation in comparison to the non-injured controls (control 16.91 ± 14.22 ms, $n = 9$ cells; 7-days post

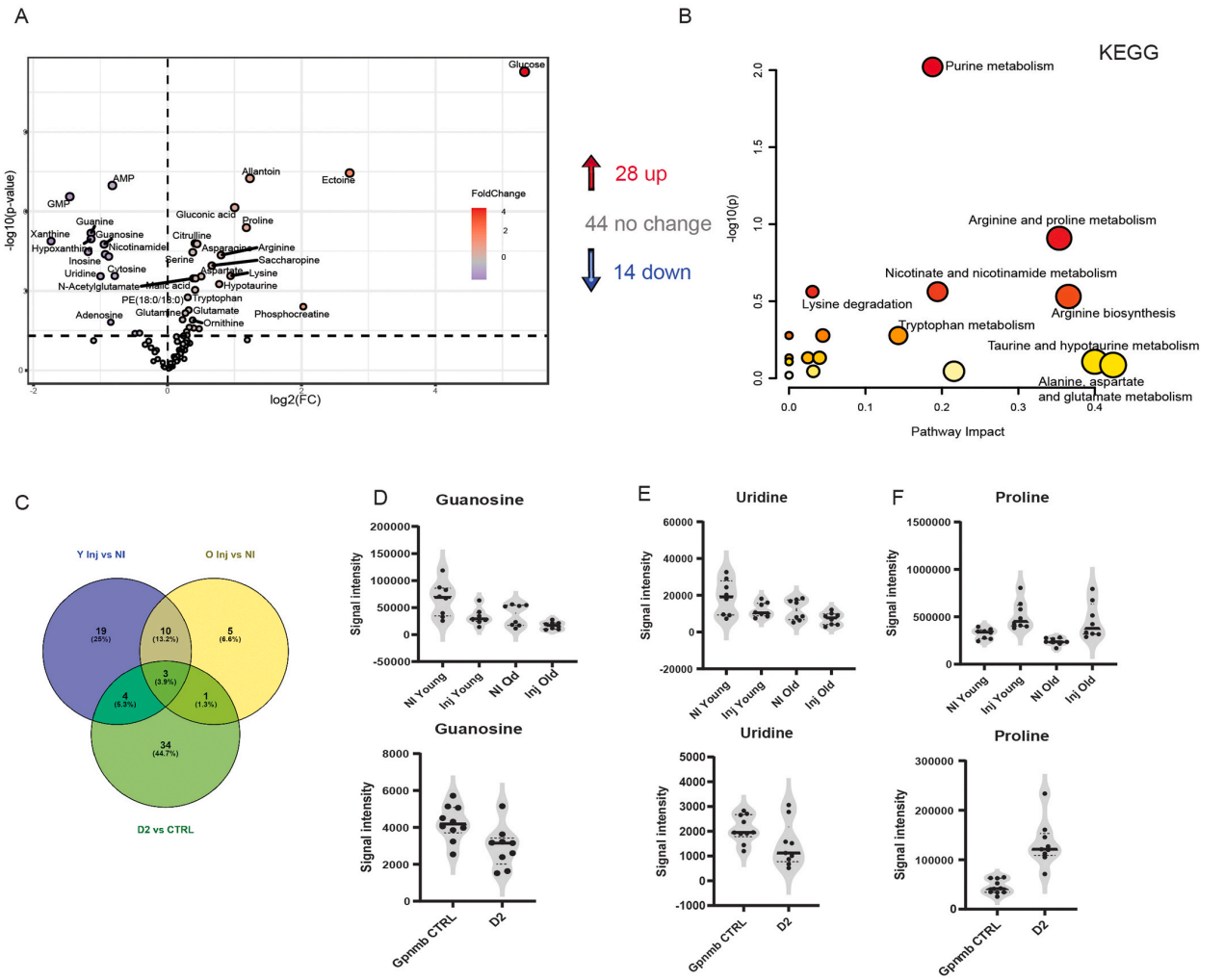

Fig. 5. Metabolic changes in other IOP models prior to RGC neurodegeneration. A: Whole retina samples of 9 months of age DBA/2J mice displaying elevated IOP without obvious RGC or axonal loss and 9 months of age Gpnmb+ control mice (CTRL) underwent metabolic profiling. In total 86 metabolites were detected. Of these, 28 metabolites were found in significantly higher levels in the retina DBA/2J mice (D2) and 14 metabolites were found with significantly lower levels in the retina of DBA/2J mice in comparison to the CTRLs, as demonstrated in the volcano plot (p-value < 0.05, red = increased, blue = decreased). 44 of the measured metabolites were not significantly altered. B: Kyoto Encyclopedia of Genes and Genomes (KEGG) pathway analysis of metabolites demonstrates significant pathway enrichment e.g. of pathways related to Purine metabolism, Nicotinate and nicotinamide metabolism, taurine and hypotaurine metabolism as well as Arginine metabolism. C: Venn diagram comparing significantly changed metabolites found in 12 months of age injured retina in comparison to 12 months of age non-injured retina, 3 months of age injured retina in comparison to 3 months of age non-injured retina and the metabolites significantly differently regulated in D2 mice vs CTRL. Three metabolites were detected in all 3 injury groups and are shown in D, E and F. D: Guanosine is found in decreased levels in all 3 groups with IOP elevation. E: Uridine is found in decreased levels after an acute IOP and chronic elevation and F: Proline was increased in the retinae of both young and old mice after single IOP injury and after chronic IOP increase. Violin plots show the non-normalized signal intensities. The black bar shows the median, the dotted lines show the 1st and the 3rd quartile.

IOP elevation 3.29 ± 3.52 ms, n = 7 cells, p-value <0.05) (Fig. 4F). sIPSCs were also measured in the non-injured control retina as well as day 3 post IOP elevation. Whereas the amplitude remained stable between the two groups (control 41.92 ± 8.73 pA, n = 4 cells; 3-days post IOP elevation 33.26 ± 2.48 pA, n = 4 cells, p-value=0.23), a significant decrease in sIPSC frequency was recoded at day 3 after IOP elevation (control 12.89 ± 4.47 Hz, n = 4 cells; 3-days post IOP elevation 3.096 ± 1.44 Hz, n = 4 cells; p-value <0.01) (Fig. 4G).

5.5. Comparison of metabolic profile in DBA/2J mice vs. short-term experimental IOP elevation

The DBA/2J (D2) mouse develops chronic IOP elevation with age due to a progressive iris disease. We assessed whether there are key differences in the retinal metabolome of whole retina samples of 9 months of age D2 mice, displaying elevated IOP without obvious RGC or axonal loss, and 9 months of age D2-Gpnmb+ control mice (dataset can be found in the source publication (Harder et al., 2020)). Of the 86 metabolites, 28 were significantly higher in D2 mice and 14 metabolites significantly lower (Fig. 5A). 20 metabolites were found in both the single-IOP elevation datasets and the D2 dataset but were not significantly altered in all three. Examples are glutamine, which was increased with IOP elevation in the D2 mice as well as the 3 months of age mice and adenosine and AMP, which are both down-regulated in 3 months of age mice and D2 mice with IOP elevation. KEGG pathway analysis of metabolites demonstrates significant pathway enrichment *e.g.* of pathways related to purine metabolism, nicotinate and nicotinamide metabolism, taurine and hypotaurine metabolism (Fig. 5B). The comparison of these altered metabolites with metabolites changed in the retina of 12 months of age or 3 months of age mice after a single IOP injury showed that 3 metabolites were altered in all 3 injury groups (Fig. 5C). Guanosine and uridine were significantly decreased in all injury groups (Fig. 5D and E) and proline was significantly increased (Fig. 5F).

Taken together, these data indicate that retinal neurotransmitters are altered with aging and following IOP elevation. The underlying mechanisms and impact of this on age-related vulnerability to IOP and glaucoma are still to be determined.

6. Discussion

Advancing age induced clear changes in the metabolite profiles of the mouse retina with significant changes in the glutamate and GABA signaling pathways. IOP elevation led to a further reduction in GABA levels and altered glutamate metabolism both after short-term IOP elevation as well as in response to long term IOP elevation in the DBA/2J mouse. This is especially interesting as glutamate and GABA are the main neurotransmitters that drive excitatory and inhibitory inputs into RGCs.

Indoxyl sulfate was the metabolite most changed with age. Indoxyl sulfate has been shown to promote neuroinflammation and oxidative stress but also decreases GABA receptors in the brain (Sun et al., 2021). This was supported by reduced levels of GABA in the 12 months of age retina. We also observed significant alterations in the biosynthesis and degradation pathways of the branch chain amino acids valine, leucine and isoleucine which were enriched in the aging retina. These amino acids are involved in glutamate production and maintenance, and disbalance can lead to oxidative stress in the retina (Lieth et al., 2001; Ola et al., 2019). These amino acids can also promote neuroprotection after traumatic brain injury by possibly buffering and maintaining correct levels of synaptic glutamate and GABA (Cole et al., 2010). In addition, a recent study demonstrating a reduction of GABAergic amacrine cells in the aging retina, underlining our analysis of lower levels of GABA in the aged retina (Zhou et al., 2024).

Sarcosine and L-lysine levels were also decreased with age and impact glutamate signaling. Sarcosine is an inhibitor of glycine 1 transporter and enhances NMDA receptor signaling by increasing extracellular glycine (Hanuska et al., 2016). By limiting excitotoxic glutamate, sarcosine was shown to promote neuroprotection in a model of oxygen/glucose deprivation of the rat hippocampus (Pinto et al., 2012). L-lysine is relevant for glutamine metabolism and is a glutamate precursor (Xiao et al., 2018). It therefore can influence glutamate levels in the CNS (Papes et al., 2001), and also inhibit excitotoxic glutamate signaling (Kondoh et al., 2010). Lysine can additionally serve as fuel source for glucose deprived brain astrocytes (Harders et al., 2024). GWAS analysis studying two glaucoma cohorts have linked several genes involved in the lysine degradation pathway to primary open angle glaucoma (*GLT25D2, EHMTA, ALDH2 and ALDH3A2)* (Bailey et al., 2014).

IOP elevation was seen to further impact the effect of advancing age on retinal metabolites. Both GABA and taurine expression was significantly decreased after IOP elevation. GABA is the main inhibitory neurotransmitter of the retina with taurine, the most abundant amino acid in the retina, acting as GABA mimetic (Garcia-Ayuso et al., 2024). GABAergic signals play an important role in shaping neuronal response patterns and reducing RGC output frequency and RGC excitability (Wang et al., 2007). We found significantly lower levels of GABA in the injured retina (compared to non-injured retina) of both 3 months of age and 12 months of age mice. This was further evidenced by a reduced numbers of GABA-expressing cells in the immunohistochemistry analysis. We detected GABA positive cells in the RGC as well as the ONL layer of the retina. GABA-hi cells resemble starburst amacrine cells, which normally reside within the INL, however can also be displaced and then appear in the GCL, where they account for approximately 12 % of the total somas (Jeon et al., 1998). GABA-lo cells within the GCL are most likely RGCs, that can show a varied range of GABA signal within the cell population (Marc and Jones, 2002), whereas GABA-lo cells in the INL represent different types of amacrine cells that can be found in the retina (Anderson et al., 2011). Reduction of eIPSC amplitude and sIPSC frequency day 3 after IOP injury further point towards reduced levels of GABA and its related receptors. There is a direct relationship between IPSC amplitude and GABA receptor numbers (Aizenman et al., 1998). Previous studies have also demonstrated a reduction in $GABA_A$ receptors with chronic IOP elevation (Lam et al., 2003; Zhou et al., 2017). The reduction of sIPSC frequency further points to a decrease in GABA release following IOP elevation, and similar changes have been demonstrated following chronic IOP elevation (Zhou et al., 2019). Interestingly, untargeted analysis of 2 large glaucoma GWAS datasets showed alterations in genes involved in GABA metabolism in primary open angle glaucoma (Bailey et al., 2014). In addition, a recently published study evaluating neural specificity in the visual cortex showed decreasing levels of GABA in the visual cortex of glaucoma patients which could be correlated to deteriorating neural specificity in the visual cortex (Bang et al., 2023).

Changes in taurine levels have also been demonstrated in several glaucoma animal models, and studies analyzing the metabolome of the aqueous humor found decreased levels of taurine in glaucoma patients (Buisset et al., 2019; Froger et al., 2012). Mice subjected to increased IOP with supplements including homotaurine, a taurine analog, significant improvement of the inner–retina derived photopic negative response (PhNR) signal in the ERG was detected (Cammalleri et al., 2020). Our analysis further shows the increase guanidoacetic acid and 4-guanidinobutanoic acid in the retina of 3 months of age, but not 12 months of age mice after IOP elevation. Both guanidoacetic acid and 4-guanidinobutanoic acid can act as a GABA mimetic and can evoke neuronal $GABA_A$ receptor mediated currents (Meera et al., 2023). We hypothesize that this could be a compensatory mechanism involved in the retina of young mice, which is absent in the retina of 12 months of age mice after IOP injury.

The changes of metabolites found in all three metabolite measurements after IOP elevation (in the 3 months of age mice and the 12 months of age mice data generated here and the publicly available metabolomics dataset using the DBA/2J mouse model (Harder et al.,

2020)) point towards a potential increase in glutamate in the retina of eyes subjected to either short or long-term IOP elevation. Guanosine, which was found in reduced levels, is a purine nucleoside which has neurotrophic and anti-apoptotic effects, mediated by its ability to stimulate neuroprotective factors from astrocytes. Guanosine is also involved in the clearance of excess glutamate from the synaptic cleft into astrocytes. This mechanism is understood to be age-dependent (Bettio et al., 2016). Uridine, also reduced in the retina after IOP elevation, is also known to alter glutaminergic synaptic transmission and plasticity and promotes neuroprotective effects. Although the exact mechanism is still unknown, uridine has shown protective and positive effects on diseases related to excess glutamate such as depression or traumatic brain injury and stroke (Chang et al., 2019). L-Proline on the other hand was increased in the retina after IOP elevation and is a non-essential amino acid neuromodulator and a known neural metabotoxin (Nadler et al., 1988). It is an agonist of glycine and glutamate receptors (Henzi et al., 1992) and additionally can induce oxidative stress in the CNS (Delwing et al., 2003).

Our results demonstrate significant alterations of retinal metabolites with age and after IOP injury. One limitation of this study is that it was restricted to a pre-defined set of metabolites. We therefore cannot provide a comprehensive overview of all metabolic pathways in the retina. Although measuring the whole retina can bring value, performing cell type specific metabolomics would provide greater resolution with respect to the identification of disease specific pathways. Despite this limitation, we could detect alterations to glaucoma-relevant neurotransmitters such as GABA and we could confirm our results with 2 independent methods. Of course, these experiments were performed in mouse models and can therefore only always in parts represent the human disease.

7. Conclusions

We believe our data will provide a useful resource for researchers studying the metabolomic consequences of age and IOP injury. Good discrimination between young and middle-aged retina was possible with the panel of metabolites measured in this study. The changes detected here support an alteration/decrease of glutamate and GABA signaling with aging, as well as in pre-apoptotic, functionally impaired, but fully recoverable RGCs following IOP injury. Reduction of GABA after IOP injury points towards a loss of inhibitory neurotransmission in the retina, which possibly is compensated in the young mice by increasing GABA-mimetics in the retina.

Ethics approval

All breeding and experimental procedures were undertaken in accordance with the Association for Research for Vision and Ophthalmology Statement for the Use of Animals in Ophthalmic and Research and were approved by the SingHealth Institutional Animal Care and Use Committee (2019/SHS/1534). Experiments for electrophysiology were performed at the Florey Institute, Melbourne, under the guidelines of the Australian Code of Practice for the Care and were approved by The Florey Animal Ethics Committee (18–112-FINMH).

Funding

PAW is supported by Karolinska Institutet in the form of a Board of Research Faculty Funded Career Position, by St. Erik Eye Hospital philanthropic donations, and Vetenskapsrådet 2022–00799. JGC is supported by the EOLAS foundation, Australia. KB was supported by a NMRC Clinician scientist individual research grant (CS-IRG NIG) grant. JCG is supported within a CRP grant National Research Foundation Singapore (CRP24–2020–0077).

CRediT authorship contribution statement

Jones Bryan W: Writing – review & editing, Validation, Methodology, Data curation. **Williams Pete A:** Writing – review & editing, Supervision, Methodology, Data curation, Conceptualization. **Crowston Jonathan G:** Writing – review & editing, Supervision, Methodology, Funding acquisition, Conceptualization. **Bell Katharina C.:** Writing – review & editing, Writing – original draft, Investigation, Formal analysis, Data curation, Conceptualization. **Chrysostomou Vicki:** Writing – review & editing, Methodology, Conceptualization. **Karlsson Markus:** Methodology.

Declaration of Competing Interest

The authors declare that they have no competing interests.

Acknowledgements

The authors would like to thank the Swedish Metabolomics Centre for performing the metabolomics analysis.

Appendix A. Supporting information

Supplementary data associated with this article can be found in the online version at doi:10.1016/j.neurobiolaging.2025.03.004.

Data availability

All raw data is available from Zenodo, doi: 10.5281/zenodo.14723294. Supplementary Dataset 1 available from the same doi contains the processed and annotated data.

References

Aizenman, C.D., et al., 1998. Polarity of long-term synaptic gain change is related to postsynaptic spike firing at a cerebellar inhibitory synapse. Neuron 21 (4), 827–835. https://doi.org/10.1016/s0896-6273(00)80598-x.

Anderson, J.R., et al., 2011. Exploring the retinal connectome. Mol. Vis. 17, 355–379.

Bailey, J.N., et al., 2014. Hypothesis-independent pathway analysis implicates GABA and acetyl-CoA metabolism in primary open-angle glaucoma and normal-pressure glaucoma. Hum. Genet 133 (10), 1319–1330. https://doi.org/10.1007/s00439-014-1468-7.

Baltan, S., et al., 2010. Metabolic vulnerability disposes retinal ganglion cell axons to dysfunction in a model of glaucomatous degeneration. J. Neurosci. 30 (16), 5644–5652. https://doi.org/10.1523/JNEUROSCI.5956-09.2010.

Bang, J.W., et al., 2023. GABA decrease is associated with degraded neural specificity in the visual cortex of glaucoma patients. Commun. Biol. 6 (1), 679. https://doi.org/10.1038/s42003-023-04918-8.

Bengtsson, B., et al., 2024. Comparison of disease severity in glaucoma patients identified by screening in the 1990s and in routine clinical care in the 2010s in Sweden. Acta Ophthalmol. 102 (2), 238–245. https://doi.org/10.1111/aos.15777.

Bettio, L.E., et al., 2016. Guanosine and its role in neuropathologies. Purinergic Signal 12 (3), 411–426. https://doi.org/10.1007/s11302-016-9509-4.

Buisset, A., et al., 2019. Metabolomic profiling of aqueous humor in glaucoma points to taurine and spermine deficiency: findings from the eye-d study. J. Proteome Res 18 (3), 1307–1315. https://doi.org/10.1021/acs.jproteome.8b00915.

Cammalleri, M., et al., 2020. A dietary combination of forskolin with homotaurine, spearmint and B vitamins protects injured retinal ganglion cells in a rodent model of hypertensive glaucoma. Nutrients 12 (4). https://doi.org/10.3390/nu12041189.

Canovai, A., et al., 2023. Pyrroloquinoline quinone drives ATP synthesis in vitro and in vivo and provides retinal ganglion cell neuroprotection. Acta Neuropathol. Commun. 11 (1), 146. https://doi.org/10.1186/s40478-023-01642-6.

Casson, R.J., et al., 2021. Retinal energy metabolism in health and glaucoma. Prog. Retin Eye Res 81, 100881. https://doi.org/10.1016/j.preteyeres.2020.100881.

Chang, E.H., et al., 2019. Assessment of glutamatergic synaptic transmission and plasticity in brain slices: relevance to bioelectronic approaches. Bioelectron. Med 5, 6. https://doi.org/10.1186/s42234-019-0022-2.

Chrysostomou, V., et al., 2014. Forced exercise protects the aged optic nerve against intraocular pressure injury. Neurobiol. Aging 35 (7), 1722–1725. https://doi.org/10.1016/j.neurobiolaging.2014.01.019.

Chrysostomou, V., et al., 2024. A new model of axon degeneration in the mouse optic nerve using repeat intraocular pressure challenge. Exp. Eye Res. 238, 109722. https://doi.org/10.1016/j.exer.2023.109722.

Chrysostomou, V., Crowston, J.G., 2013. The photopic negative response of the mouse electroretinogram: reduction by acute elevation of intraocular pressure. Invest Ophthalmol. Vis. Sci. 54 (7), 4691–4697. https://doi.org/10.1167/iovs.13-12415.

Cole, J.T., et al., 2010. Dietary branched chain amino acids ameliorate injury-induced cognitive impairment. Proc. Natl. Acad. Sci. USA 107 (1), 366–371. https://doi.org/10.1073/pnas.0910280107.
Covarrubias, A.J., et al., 2021. NAD(+) metabolism and its roles in cellular processes during ageing. Nat. Rev. Mol. Cell Biol. 22 (2), 119–141. https://doi.org/10.1038/s41580-020-00313-x.
Crowston, J.G., et al., 2015. An acute intraocular pressure challenge to assess retinal ganglion cell injury and recovery in the mouse. Exp. Eye Res 141, 3–8. https://doi.org/10.1016/j.exer.2015.03.006.
Delwing, D., et al., 2003. Proline induces oxidative stress in cerebral cortex of rats. Int J. Dev. Neurosci. 21 (2), 105–110. https://doi.org/10.1016/s0736-5748(02)00109-0.
van den Berg, R.A., et al., 2006. Centering, scaling, and transformations: improving the biological information content of metabolomics data. BMC Genom. 7, 142. https://doi.org/10.1186/1471-2164-7-142.
Froger, N., et al., 2012. Taurine provides neuroprotection against retinal ganglion cell degeneration. PLoS One 7 (10), e42017. https://doi.org/10.1371/journal.pone.0042017.
Fry, L.E., et al., 2018. The coma in glaucoma: Retinal ganglion cell dysfunction and recovery. Prog. Retin Eye Res 65, 77–92. https://doi.org/10.1016/j.preteyeres.2018.04.001.
Garcia-Ayuso, D., et al., 2024. Taurine: a promising nutraceutic in the prevention of retinal degeneration. Neural Regen. Res 19 (3), 606–610. https://doi.org/10.4103/1673-5374.380820.
GBD 2019 Blindness and Vision Impairment Collaborators, Vision Loss Expert Group of the Global Burden of Disease Study, 2021. Causes of blindness and vision impairment in 2020 and trends over 30 years, and prevalence of avoidable blindness in relation to VISION 2020: the Right to Sight: an analysis for the Global Burden of Disease Study. Lancet Glob. Health 9 (2), e144–e160. https://doi.org/10.1016/S2214-109X(20)30489-7.
Hanuska, A., et al., 2016. Some operational characteristics of glycine release in rat retina: the role of reverse mode operation of glycine transporter Type-1 (GlyT-1) in ischemic conditions. Neurochem. Res 41 (1-2), 73–85. https://doi.org/10.1007/s11064-015-1713-z.
Harder, J.M., et al., 2020. Disturbed glucose and pyruvate metabolism in glaucoma with neuroprotection by pyruvate or rapamycin. Proc. Natl. Acad. Sci. USA 117 (52), 33619–33627. https://doi.org/10.1073/pnas.2014213117.
Harders, A.R., et al., 2024. Exogenous substrates prevent the decline in the cellular ATP content of primary rat astrocytes during glucose deprivation. Neurochem. Res 49 (5), 1188–1199. https://doi.org/10.1007/s11064-024-04104-0.
Henzi, V., et al., 1992. L-proline activates glutamate and glycine receptors in cultured rat dorsal horn neurons. Mol. Pharm. 41 (4), 793–801.
Jeon, C.J., et al., 1998. The major cell populations of the mouse retina. J. Neurosci. 18 (21), 8936–8946. https://doi.org/10.1523/JNEUROSCI.18-21-08936.1998.
Kondoh, T., et al., 2010. Lysine and arginine reduce the effects of cerebral ischemic insults and inhibit glutamate-induced neuronal activity in rats. Front. Integr. Neurosci. 4 (18). https://doi.org/10.3389/fnint.2010.00018.
Kong, Y.X., et al., 2009. Functional changes in the retina during and after acute intraocular pressure elevation in mice. Invest. Ophthalmol. Vis. Sci. 50 (12), 5732–5740. https://doi.org/10.1167/iovs.09-3814.
Lam, D.Y., et al., 2003. Neurochemical correlates of cortical plasticity after unilateral elevated intraocular pressure in a primate model of glaucoma. Invest Ophthalmol. Vis. Sci. 44 (6), 2573–2581. https://doi.org/10.1167/iovs.02-0779.
Lieth, E., et al., 2001. Nitrogen shuttling between neurons and glial cells during glutamate synthesis. J. Neurochem. 76 (6), 1712–1723. https://doi.org/10.1046/j.1471-4159.2001.00156.x.
Marc, R.E., et al., 1995. Pattern recognition of amino acid signatures in retinal neurons. J. Neurosci. 15 (7 Pt 2), 5106–5129. https://doi.org/10.1523/JNEUROSCI.15-07-05106.1995.
Marc, R.E., Jones, B.W., 2002. Molecular phenotyping of retinal ganglion cells. J. Neurosci. 22 (2), 413–427. https://doi.org/10.1523/JNEUROSCI.22-02-00413.2002.
Meera, P., et al., 2023. Guanidinoacetate (GAA) is a potent GABA(A) receptor GABA mimetic: Implications for neurological disease pathology. J. Neurochem. 165 (3), 445–454. https://doi.org/10.1111/jnc.15774.
Mir, C., et al., 2003. CDP-choline prevents glutamate-mediated cell death in cerebellar granule neurons. J. Mol. Neurosci. 20 (1), 53–60. https://doi.org/10.1385/JMN:20:1:53.
Myer, C., et al., 2020. Differentiation of soluble aqueous humor metabolites in primary open angle glaucoma and controls. Exp. Eye Res. 194, 108024. https://doi.org/10.1016/j.exer.2020.108024.
Nadler, J.V., et al., 1988. Toxicity of L-proline toward rat hippocampal neurons. Brain Res. 456 (1), 168–172. https://doi.org/10.1016/0006-8993(88)90358-7.
Ola, M.S., et al., 2019. Gabapentin attenuates oxidative stress and apoptosis in the diabetic rat retina. Neurotox. Res. 36 (1), 81–90. https://doi.org/10.1007/s12640-019-00018-w.
Papes, F., et al., 2001. The essential amino acid lysine acts as precursor of glutamate in the mammalian central nervous system. FEBS Lett. 488 (1-2), 34–38. https://doi.org/10.1016/s0014-5793(00)02401-7.
Pinto, M.C., et al., 2012. Pharmacological induction of ischemic tolerance in hippocampal slices by sarcosine preconditioning. Neurochem. Int. 61 (5), 713–720. https://doi.org/10.1016/j.neuint.2012.06.018.
Quigley, H.A., Broman, A.T., 2006. The number of people with glaucoma worldwide in 2010 and 2020. Br. J. Ophthalmol. 90 (3), 262–267. https://doi.org/10.1136/bjo.2005.081224.
Rossi, C., et al., 2019. Multi-omics approach for studying tears in treatment-naive glaucoma patients. Int. J. Mol. Sci. 20 (16). https://doi.org/10.3390/ijms20164029.
Schnackenberg, L.K., et al., 2007. Metabonomics evaluations of age-related changes in the urinary compositions of male Sprague Dawley rats and effects of data normalization methods on statistical and quantitative analysis. BMC Bioinforma. 8 7 (7), S3. https://doi.org/10.1186/1471-2105-8-S7-S3.
Schousboe, A., et al., 2013. Astrocytic control of biosynthesis and turnover of the neurotransmitters glutamate and GABA. Front. Endocrinol. 4, 102. https://doi.org/10.3389/fendo.2013.00102.
Sun, C.Y., et al., 2021. Indoxyl sulfate caused behavioral abnormality and neurodegeneration in mice with unilateral nephrectomy. Aging (Albany NY) 13 (5), 6681–6701. https://doi.org/10.18632/aging.202523.
Tan, J.K., et al., 2023. Metabolomics profiling of age-associated metabolites in malay population. Oxid. Med. Cell Longev. 2023, 4416410. https://doi.org/10.1155/2023/4416410.
Tham, Y.C., et al., 2014. Global prevalence of glaucoma and projections of glaucoma burden through 2040: a systematic review and meta-analysis. Ophthalmology 121 (11), 2081–2090. https://doi.org/10.1016/j.ophtha.2014.05.013.
Tribble, J.R, et al., 2021. Nicotinamide provides neuroprotection in glaucoma by protecting against mitochondrial and metabolic dysfunction. Redox Biol. 43, 101988. https://doi.org/10.1016/j.redox.2021.101988.
Wang, C.T., et al., 2007. GABA(A) receptor-mediated signaling alters the structure of spontaneous activity in the developing retina. J. Neurosci. 27 (34), 9130–9140. https://doi.org/10.1523/JNEUROSCI.1293-07.2007.
Wang, Y., et al., 2018. Metabolic signature of the aging eye in mice. Neurobiol. Aging 71, 223–233. https://doi.org/10.1016/j.neurobiolaging.2018.07.024.
Williams, P.A., et al., 2017. Vitamin B(3) modulates mitochondrial vulnerability and prevents glaucoma in aged mice. Science 355 (6326), 756–760. https://doi.org/10.1126/science.aal0092.
Wyczalkowska-Tomasik, A., et al., 2017. Age-dependent increase in serum levels of indoxyl sulphate and p-cresol sulphate is not related to their precursors: tryptophan and tyrosine. Geriatr. Gerontol. Int. 17 (6), 1022–1026. https://doi.org/10.1111/ggi.12811.
Xia, J., et al., 2009. MetaboAnalyst: a web server for metabolomic data analysis and interpretation. Nucleic Acids Res. 37 (WebServer), W652–660. https://doi.org/10.1093/nar/gkp356.
Xia, J., Wishart, D.S., 2011. Web-based inference of biological patterns, functions and pathways from metabolomic data using MetaboAnalyst. Nat. Protoc. 6 (6), 743–760. https://doi.org/10.1038/nprot.2011.319.
Xiao, C.W., et al., 2018. Dietary L-lysine supplementation altered the content of pancreatic polypeptide, enzymes involved in glutamine metabolism, and beta-actin in rats. Amino Acids 50 (12), 1729–1737. https://doi.org/10.1007/s00726-018-2648-x.
Yoon, S.J., et al., 2009. Decreased glutamate/glutamine levels may mediate cytidine's efficacy in treating bipolar depression: a longitudinal proton magnetic resonance spectroscopy study. Neuropsychopharmacology 34 (7), 1810–1818. https://doi.org/10.1038/npp.2009.2.
Zhang, X., et al., 2023. Branched-chain amino acids metabolism and their roles in retinopathy: from relevance to mechanism. Nutrients 15 (9). https://doi.org/10.3390/nu15092161.
Zhou, X., et al., 2017. Differential modulation of GABA(A) and NMDA receptors by an alpha7-nicotinic acetylcholine receptor agonist in chronic glaucoma. Front. Mol. Neurosci. 10, 422. https://doi.org/10.3389/fnmol.2017.00422.
Zhou, X., et al., 2019. Quercetin enhances inhibitory synaptic inputs and reduces excitatory synaptic inputs to OFF- and ON-type retinal ganglion cells in a chronic glaucoma rat model. Front Neurosci. 13, 672. https://doi.org/10.3389/fnins.2019.00672.
Zhou, Y., et al., 2024. Dysregulated energy and protein homeostasis and the loss of GABAergic amacrine cells in aging retina. Exp. Eye Res. 245, 109985. https://doi.org/10.1016/j.exer.2024.109985.